ACTIVE CONTROL STRATEGIES FOR VIBRATION ISOLATION

Brad M. Beadle[1], Stefan Hurlebaus[2], Lothar Gaul[1], Uwe Stöbener[3]
[1]*Institute A of Mechanics, University of Stuttgart, Allmandring 5 b,70550 Stuttgart, Germany;*
[2]*Dept. of Civil Engineering, Texas A&M University, College Station, TX, 77843-3136, USA;*
[3]*Halcyonics GmbH, Tuchmacherweg 12, 37079 Göttingen, Germany*

Abstract: In the fields of high-resolution metrology and manufacturing, effective anti-vibration measures are required to obtain precise and repeatable results. This is particularly true when the amplitudes of ambient vibration and the dimensions of the investigated or manufactured structure are comparable, e.g. in sub-micron semiconductor chip production, holographic interferometry, confocal optical imaging, and scanning probe microscopy. In the active anti-vibration system examined, signals are acquired by extremely sensitive vibration detectors, and the vibration is reduced using a feedback controller to drive electrodynamic actuators. This paper deals with the modeling and control of this anti-vibration system. First, a six-degree-of-freedom rigid body model of the system is developed. The unknown parameters of the unloaded system, including actuator transduction constants, spring stiffness, damping, moments of inertia, and the vertical position of the center of mass, are determined by comparing measured transfer functions to those calculated using the updated model. Finally, two different strategies for actively controlling the vibration isolation system are considered.

Keywords: Active vibration isolation, MIMO control, parameter identification, SISO control, six-degree of-freedom rigid body

1. INTRODUCTION

Isolating a piece of delicate equipment from the vibration of a base structure is of practical importance in a number of engineering fields. The quest for tighter production tolerances and higher resolution has led to more stringent requirements regarding ambient vibration levels. In the majority of cases, the base supporting a piece of precision equipment is flexible and vibrates with an unpredictable waveform containing significant energy over a broad range of frequencies. The active isolation of equipment from a vibrating base structure is considered in this paper. Passive anti-vibration

mounts are widely used to isolate precision equipment from base vibration. Although conventional passive mounts offer good isolation at high frequencies, they suffer from vibration amplification at the mounted resonance frequency. Generally, the best isolation performance is achieved by using an active system in combination with a passive mount, whereby the fundamental mounted resonance can be actively controlled without compromising the high frequency performance.

Relevant active vibration isolation techniques can be found in several recent publications[1-5]. This paper investigates a commercially available six-degree-of-freedom (DOF) active vibration isolation system. Active vibration isolation is achieved in the as-built system using a decentralized control scheme consisting of independent, analog "SISO" (single input, single output) controllers. The ultimate goal of the study is to investigate alternative controllers, such as the "MIMO" (multiple input, multiple output) controller, for use in vibration isolation. However, successful implementation of such controllers first requires an accurate physical model of the vibration isolation system. In section 2, a six-DOF rigid body model of the unloaded vibration isolation system is developed. In section 3, model parameters associated with the unloaded vibration isolation system are determined using experimentally measured transfer functions. In section 4, the SISO- and MIMO- control strategies are discussed.

2. MODELING

2.1 System Model

The vibration isolation system is essentially composed of two plates connected by springs and actuators. A physical model of the vibration isolation system is depicted in figure 1. Assuming that the motion of the upper plate undergoes rigid body motion only, then its motion can be described using six coordinates. Referring to the upper plate, the coordinates x, y, and z are used to describe the linear motion of the plate, and the coordinates ϕ_x, ϕ_y, and ϕ_z are used to describe small rotations about the x, y, and z axes, respectively. The coordinate system is located at the center of mass of the plate and is aligned with the plate's principal axes. Due to plate symmetry, the principal axes align with the geometric axes of symmetry, and the x and y coordinates of the center of mass coincide with the geometric center of the plate. In a similar fashion, the motion of the lower plate is described using the coordinates x^d, y^d, z^d, ϕ_x^d, ϕ_y^d, and ϕ_z^d.

The upper plate is suspended above the lower plate with four springs, each of which is denoted by the stiffness k_s. The physical model contains additional stiffnesses, namely k_t and k_r, to model the transverse and rotational

stiffness, respectively, associated with the suspension springs. Presumably, the motion of the lower plate is identical to the motion of the surface upon which the vibration isolation system rests. The coordinates describing the motion of the lower plate can therefore be viewed as disturbance inputs. The motion of the lower plate is coupled to the upper plate via the suspension, transverse, and rotational springs. Four vertical actuators, A_1-A_4, and four horizontal actuators, A_5-A_8, are rigidly attached to the upper plate, and interact with the lower plate via point contact. The vertical actuators can slide horizontally relative to the lower plate, and the horizontal actuators can slide vertically relative to the lower plate. Active vibration control is realized by driving the actuators with the appropriate control inputs. The coordinates L_1-L_3 are used to locate the suspension springs and the vertical actuators, and the coordinates L_4-L_6 are used to locate the horizontal actuators.

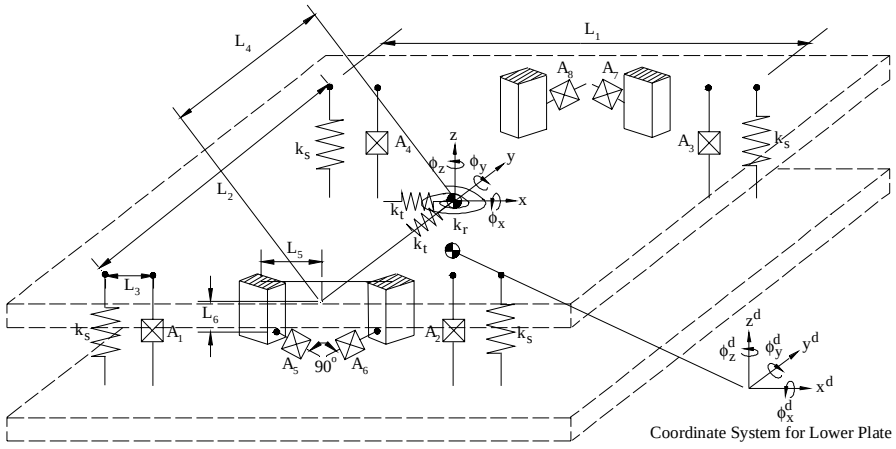

Figure 1. Physical model of the vibration isolation system.

2.2 Actuator Model

The physical model of an actuator is depicted in figure 2. The main components of the actuator are a stationary permanent magnet and a coil-wrapped reaction mass m_a which moves relative to the permanent magnet. A damper having value d_a has been included to model energy losses, and a spring having stiffness k_a has been included to model the spring-like restoring force between the permanent magnet and the reaction mass. When a voltage V is applied to the coil, a current I will flow through it. An electromotive force F proportional to the current (and therefore to the

applied voltage, assuming a purely resistive coil) is developed by the coil, thereby causing the reaction mass to accelerate.

A simplified actuator model is depicted to the right in figure 2. This is the actuator model which is implemented in the overall model for the vibration isolation system. The reaction mass has been eliminated in the simplified actuator model since its motion is totally constrained in the vibration isolation system. Additionally, the damping parameter d_a has been excluded from the simplified actuator model since its effects are negligible in comparison to other system energy loss mechanisms, such as the friction occurring at the points of contact between the lower plate and the actuators.

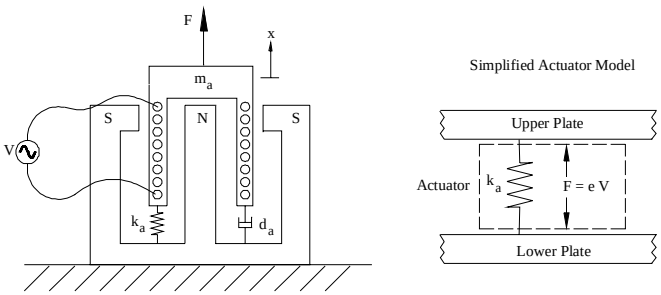

Figure 2. Physical model of an actuator.

2.3 Equations of Motion

The unloaded vibration isolation system is composed of two rigid bodies: the lower plate and the upper plate. The motion of the lower plate is presumably given, i.e., it has the same motion as the surface upon which it rests. The following equations of motion[6] can then be used to solve for the unknown motion of the upper plate:

$$\sum \overline{F} = m\overline{a}_{\mathrm{G}} \tag{1}$$

$$\sum \overline{M}_{\mathrm{G}} = \dot{\overline{H}}_{\mathrm{G}} \approx \begin{bmatrix} I_{xx} & 0 & 0 \\ 0 & I_{yy} & 0 \\ 0 & 0 & I_{zz} \end{bmatrix} \begin{Bmatrix} \ddot{\phi}_x \\ \ddot{\phi}_y \\ \ddot{\phi}_z \end{Bmatrix} \tag{2}$$

The force balance is stated in Eq. (1), where m is the mass of the upper plate, and $\overline{a}_{\mathrm{G}}$ is the acceleration of its mass center G. The moment balance is stated in Eq. (2), where $\dot{\overline{H}}_{\mathrm{G}}$ is the rate of change of angular momentum about the center of mass, and I_{xx}, I_{yy}, I_{zz} are the principle moments of inertia. The approximation in Eq. (2) is valid only for small angular displacements. The

left hand side of Eqs. (1) and (2) are determined by summing force and moment contributions, respectively, from the various springs and actuators. The resultant equations of motion for the upper plate are:

$$[M]\ddot{\bar{w}} + [D]\dot{\bar{w}} + [K]\bar{w} = [D]\dot{\bar{w}}^{\mathrm{d}} + [K]\bar{w}^{\mathrm{d}} + [E]\bar{v}, \tag{3}$$

$$\bar{w} = \{x \quad y \quad z \quad \phi_x \quad \phi_y \quad \phi_z\}^{\mathrm{T}},$$

$$\bar{w}^{\mathrm{d}} = \{x^{\mathrm{d}} \quad y^{\mathrm{d}} \quad z^{\mathrm{d}} \quad \phi_x{}^{\mathrm{d}} \quad \phi_y{}^{\mathrm{d}} \quad \phi_z{}^{\mathrm{d}}\}^{\mathrm{T}},$$

where $\bar{v}$ is the vector containing the input voltages applied to the actuators (the vector elements v_1-v_8 correspond to actuators A_1-A_8, respectively). Analysis details and expressions for the mass matrix [*M*], damping matrix [*D*], stiffness matrix [*K*], and actuator transduction matrix [*E*] are given by Beadle, et al.[7]. The analysis assumes that the damping matrix is diagonal, so that the damping of a particular rigid body mode does not depend on the motion of another rigid body mode. The individual entries of the damping matrix are determined experimentally. The first two terms on the right hand side of Eq. (3) represent the disturbance excitation due to the motion of the lower plate. The third term on the right hand side of Eq. (3) is the excitation generated by the actuators.

The transfer function *T* relating displacement at an arbitrary location and in an arbitrary direction, to force input from the r^{th} actuator has been derived by Beadle, et al.[7]. The derivation assumes forced, harmonic, steady state motion and zero disturbance inputs, $\bar{w}^{d} = 0$.

3. PARAMETER IDENTIFICATION

3.1 Experimental Setup

The experimental setup for identifying the unknown parameters in the theoretical model is depicted in figure 3. The unknown parameters include: spring stiffnesses, damping, actuator transduction constants, moments of inertia, and the vertical position of the upper plate's center of mass. The other constants required for the model are known: L_1=0.348 m, L_2=0.3 m, L_3=0.055 m, (L_4+L_5)=0.19 m, and mass m =19.3 kg. An HP Paragon measurement system is configured to drive one or more of the actuators using a random voltage excitation *V*. The excitation signal is amplified using the preamplifiers which are built into the commercial vibration isolation system. In the diagram, the vertical actuators are denoted by A_1-A_4, and the horizontal actuators are denoted by A_5-A_8. The response of the upper plate is measured using an accelerometer (Brüel & Kjær 4381) placed at one of the three measurement locations M_1-M_3. The vibration

isolation system actually has built-in accelerometers at each of the actuator locations. In future efforts, these accelerometers will be used for the parameter identification procedure. The accelerometer used in the current study can be oriented to measure acceleration in any of the three coordinate directions. The acceleration signal is converted into displacement *X* using a signal conditioner before being received by the measurement system. The measurement system then computes the *X/V* transfer function from the random displacement and voltage waveforms. Division of the measured *X*/*V* transfer function by the appropriate actuator constant e_r results in the displacement-force transfer function *X*/*F*.

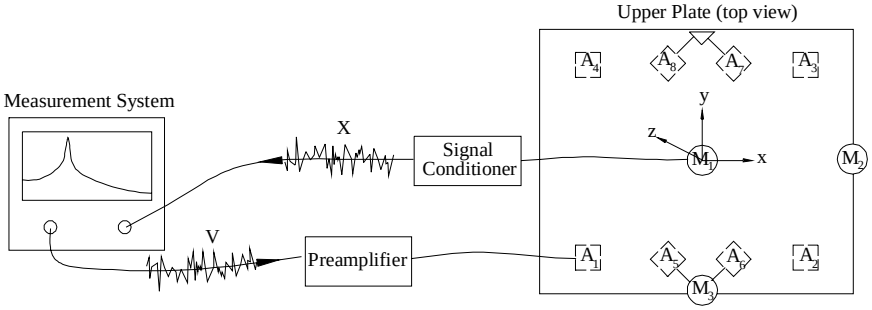

Figure 3. Experimental setup for determining model parameters.

3.2 Experimental Results

The results of the parameter identification procedure for the unloaded vibration isolation system are summarized in Table 1. In the table, the actuation constants are denoted by *e*, the damping coefficients are denoted by *d*, and the moments of inertia are denoted by *I*. A similar set of tests has been used to identify parameters for an arbitrarily loaded vibration isolation system[7]. For explicative purposes, refer to test 5 in table 1. For this test, the four actuators A_1-A_4 were driven, and the accelerometer was used to measure the motion in the *z*-direction at measurement location M_3. Actuators A_3 and A_4 were driven 180^o out of phase relative to actuators A_1 and A_2. This particular drive scheme excites pure rotational motion about the *x* axis. Hence, the unknown moment of inertia and rotational damping about this axis can be determined by comparing the measured transfer function with the theoretical transfer function. Specifically, the theoretical transfer function Z_3/F_1 is computed for several different values of I_{xx} and d_4. An error function given by

$$error = \left(\overline{T}_{\text{exp}} - \overline{T}_{\text{theo}}\right) \cdot \left(\overline{T}_{\text{exp}} - \overline{T}_{\text{theo}}\right)^{*} \tag{4}$$

is then calculated. Here, $\overline{T}_{exp}$ and $\overline{T}_{theo}$ are the experimental and theoretical transfer functions, respectively, and the * operator denotes complex conjugation of individual vector entries. The error function is calculated for values of the transfer functions in the frequency range 2.5-20 Hz. Finally, the parameter values which minimize the error function are determined.

Table 1. Parameter identification results for the unloaded vibration isolation system.

Test	Actuator	Displacement	Parameter
1	A_1	z_1	e_1 = 6.59 N/V |
2	A_2	z_1	e_2 = 7.85 N/V | k_s=11300 N/m
3	A_3	z_1	e_3 = 7.07 N/V | d_3=275 Ns/m
4	A_4	z_1	e_4 = 8.10 N/V |
5	$(A_1+ A_2)- (A_3+ A_4)$	z_3	I_{xx}=0.340 kgm^2, d_4=6.74 Ns/rad
6	$(A_1+ A_4)- (A_2+ A_3)$	z_2	I_{yy}=0.259 kgm^2, d_5=3.48 Ns/rad
7	$(A_1+ A_4)- (A_2+ A_3)$	x_1	L_6=0.054 m
8	A_5	x_1	e_5 = 7.50 N/V |
9	A_6	x_1	e_6 = 7.89 N/V | k_t=37600 N/m
10	A_7	x_1	e_7 = 6.65 N/V | d_1=279 Ns/m
11	A_8	x_1	e_8 = 5.97 N/V |
12	$A_5+ A_7$	x_3	I_{zz}=0.500 kgm^2, k_r=1590 N/rad d_6=9.32 Ns/rad

Comparison between the measured and theoretical transfer functions are depicted in figures 4-7 for selected test cases. Overall agreement between experimental and theoretical curves is good, thereby giving confidence in the physical model and the parameter identification procedure. The deviation between the curves at low frequency is caused by ground-induced motion of the lower plate and/or the limited low frequency response of the accelerometer.

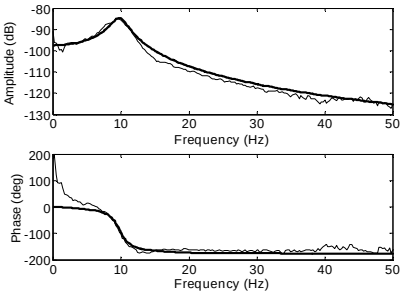

Figure 4. Experimental (—) and theoretical (▬) transfer functions for test case 1.

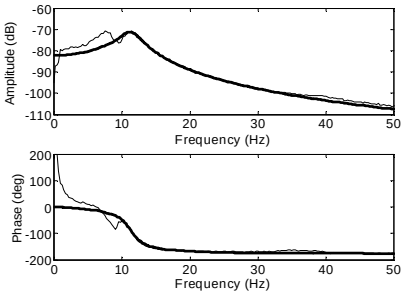

Figure 5. Experimental (—) and theoretical (▬) transfer functions for test case 5.

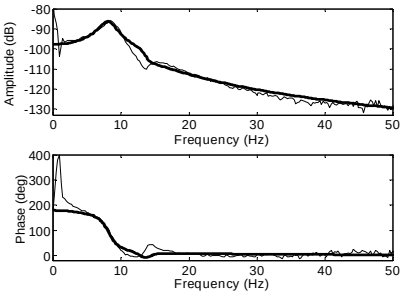

Figure 6. Experimental (—) and theoretical (▬) transfer functions for test case 8.

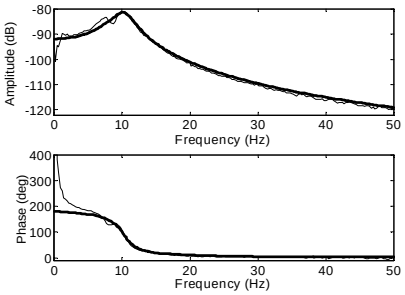

Figure 7. Experimental (—) and theoretical (▬) transfer functions for test case 12.

4. CONTROL STRATEGIES

4.1 SISO Controller

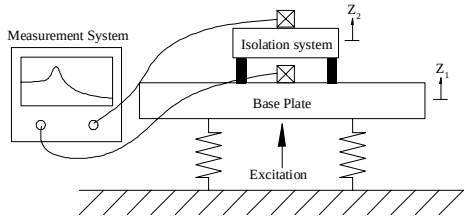

Figure 8. Experimental setup for measuring vertical transmissibility.

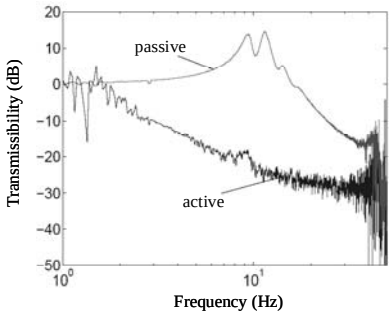

Figure 9. Measured transmissibility of the vibration isolation system with (active) and without (passive) control.

The commercial vibration isolation system implements a decentralized SISO control strategy in which each of the actuators is controlled using feedback from a local acceleration sensor. The local controllers are proportional-derivative controllers, and they are realized using analog circuitry. The performance of the as-built vibration isolation system is assessed by measuring the transmissibilty. The experimental setup for measuring vertical transmissibilty is depicted in figure 8. As shown, a large base plate is driven vertically using random excitation. The vertical motion Z_1 of the base structure and the vertical motion Z_2 of the upper plate in the vibration isolation system are measured using accelerometers. A measurement system is then used to compute the transmissibilty function Z_2/Z_1 from the measured displacements. The measured transmissibilty of

the vibration isolation system with (active) and without (passive) control are depicted in figure 9. Clearly, the vibration isolation system with analog SISO control effectively eliminates vibrations at the mounted vertical resonance frequency of ~10 Hz.

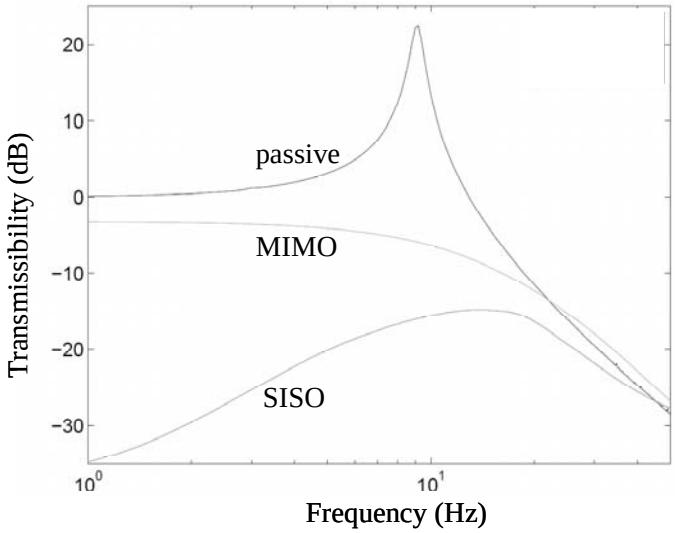

Figure 10. Simulated vertical transmissibilty curves for various control cases.

4.2 MIMO Controller

Ignoring the disturbance inputs, the equation of motion for the upper plate, Eq. (3), can be cast into state-space form:

$$\dot{\bar{x}} = [A]\bar{x} + [B]\bar{u}, \text{ with } \bar{x} = \begin{bmatrix} \bar{w} \\ \dot{\bar{w}} \end{bmatrix}, \quad \bar{u} = \bar{v}\,. \tag{5}$$

For the MIMO controller, the state feedback law $\bar{u} = -[K]\bar{x}$ is assumed. The elements in [*K*] are obtained using the pole placement method, and the elements of the state-space vector $\bar{x}$ are estimated from measured acceleration outputs using an observer[8]. Simulated transmissibility curves for passive, SISO-controlled, and MIMO-controlled systems are depicted in figure 10. The SISO controller outperforms the MIMO controller for low-frequency vertical excitation. In future simulations, the performance of the controllers will be compared for arbitrary excitation composed of vertical, horizontal, and angular disturbance inputs. At higher frequencies, the structural response is dominated by inertial effects and is therefore only minimally influenced by disturbance and control inputs. Hence, the SISO-

and MIMO- controlled systems have a similar response to the passive system at higher frequencies.

5. CONCLUSIONS

A six-DOF rigid body model for a commercially available vibration isolation system has been developed. The parameters of the unloaded vibration isolation system, including actuator transduction constants, spring stiffness, damping, moments of inertia, and the vertical position of the center of mass, were determined by comparing theoretical and measured transfer functions. The responses predicted by the model agreed well with the experimental measurements, thereby giving confidence in the model. This work is important for model-based control techniques which require accurate identification of model parameters. Future work will involve modification of the current test bed so that vertical, horizontal, and angular disturbance inputs can be used to perturb the vibration isolation system. The SISO and MIMO controllers will be experimentally compared for the various disturbance input cases. Other control concepts, including adaptive and robust control algorithms, will also be implemented and compared.

6. REFERENCES

1. C.R. Fuller, S.J. Elliott, P.A. Nelson, *Active Control of Vibration*, Academic Press, 1996.
2. U. Stöbener, L. Gaul, "Piezoelectric Stack Actuator: FE Modeling and Application for Vibration Isolation," *Proceedings of the NATO Advanced Study Institute on Responsive Systems for Active Vibration Control*, Ed. A. Preumont, Kluwer Academic Publishers, Dordecht, 2001.
3. S. Hurlebaus, *Smart Structures- Fundamentals and Applications*, Lecture Notes, Institute A of Mechanics, University of Stuttgart, 2005.
4. X. Huang, S.J. Elliott, M.J. Brennan, "Active Isolation of a Flexible Structure from Base Vibration," *Journal of Sound and Vibration*, **263**, 357-376.
5. S. Riebe, H. Ulbrich, "Modeling and Online Computation of the Dynamics of a Parallel Kinematic with Six Degrees-of-Freedom," *Archive of Applied Mechanics*, **72**, 817-829, 2003.
6. J.H. Ginsberg, *Advanced Engineering Dynamics, 2nd Ed.*, Cambridge University Press, New York, 1995.
7. B.M. Beadle, S. Hurlebaus, U. Stöbener, L. Gaul, "Modeling and Parameter Identification of an Active Anti-Vibration System," SPIE International Symposia in Smart Structures & Materials/NDE, San Diego, March 2005.
8. J. Van de Vegte, *Feedback Control Systems, 3rd Ed.*, Prentice Hall, N.J., 1994.